

Supplementary Materials for

Mechanism of calmodulin inactivation of the calcium-selective TRP channel TRPV6

Appu K. Singh, Luke L. McGoldrick, Edward C. Twomey, Alexander I. Sobolevsky*

*Corresponding author. Email: as4005@cumc.columbia.edu

Published 15 August 2018, *Sci. Adv.* **4**, eaau6088 (2018)

DOI: [10.1126/sciadv.aau6088](https://doi.org/10.1126/sciadv.aau6088)

This PDF file includes:

- Fig. S1. Overview of single-particle cryo-EM for hTRPV6-CaM.
- Fig. S2. Comparison of cryo-EM densities for hTRPV6, hTRPV6-CaM, and rTRPV6-CaM.
- Fig. S3. Cryo-EM density for hTRPV6-CaM.
- Fig. S4. Structures of CaM bound to ion channel fragments.
- Fig. S5. Overview of single-particle cryo-EM for rTRPV6-CaM.
- Fig. S6. Cryo-EM density for rTRPV6-CaM.
- Fig. S7. Comparison of hTRPV6-CaM and rTRPV6-CaM.
- Fig. S8. Sequence alignment of TRPV subunits.
- Fig. S9. Superposition of the C termini in different TRPV6 subunits.
- Fig. S10. hTRPV6 selectivity filter from different gating states.
- Table S1. Cryo-EM data collection, refinement, and validation statistics.
- Reference (42)

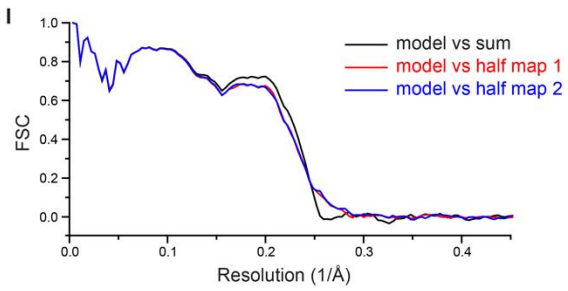
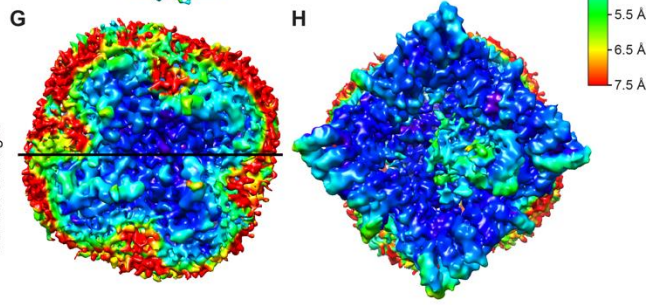
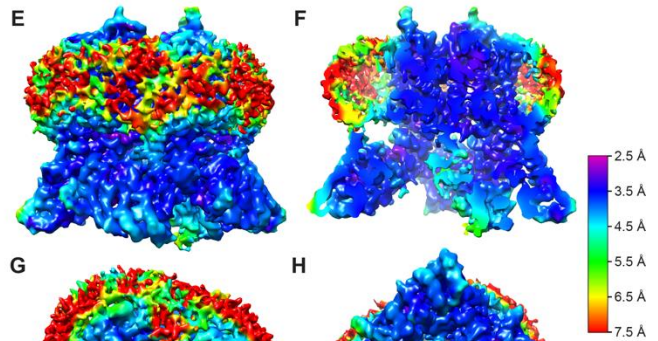
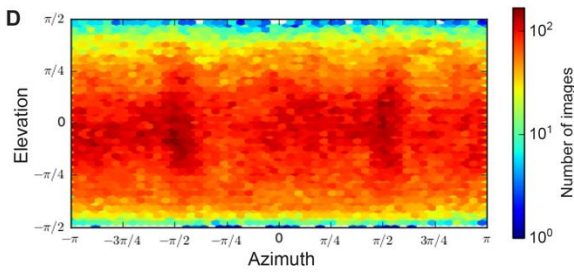
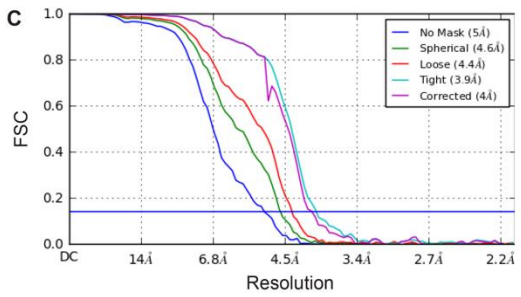
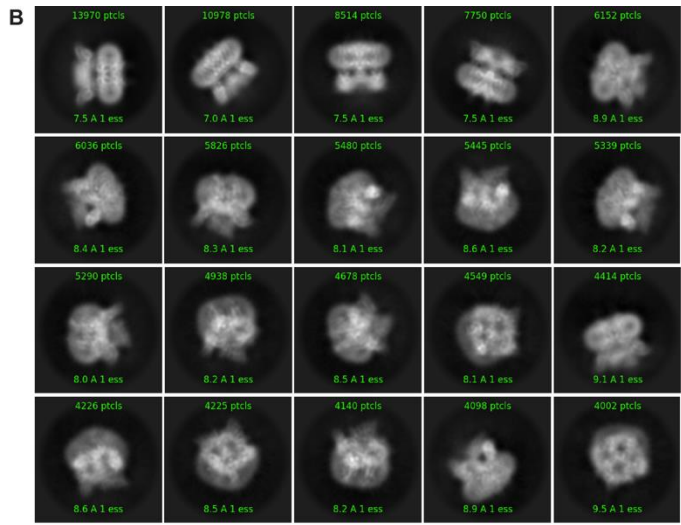
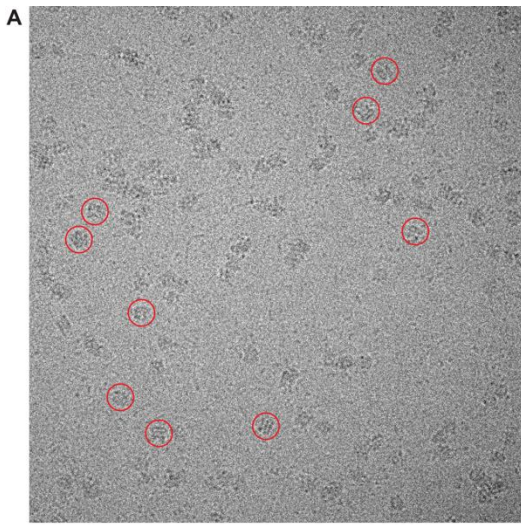


Fig. S1. Overview of single-particle cryo-EM for hTRPV6-CaM. (A) Example cryo-EM micrograph for hTRPV6-CaM with example particles circled in red. (B) Reference-free 2D class averages of hTRPV6-CaM illustrating different particle orientations. (C) Fourier shell correlation (FSC) curves from refinement. (D) Distribution of particle orientations contributing to the final 4.0 Å reconstruction. (E to H) Local resolution mapped on the hTRPV6-CaM density viewed parallel to the membrane (E and F), either in its entirety (E) or coronally halved (F) as well as viewed extracellularly (G) and intracellularly (H). The black horizontal line in (G) indicates the location of the slicing plane in (F). (I) Cross-validation FSC curves for the refined model versus unfiltered half maps (only half map1 was used for PHENIX refinement) and the unfiltered summed map.

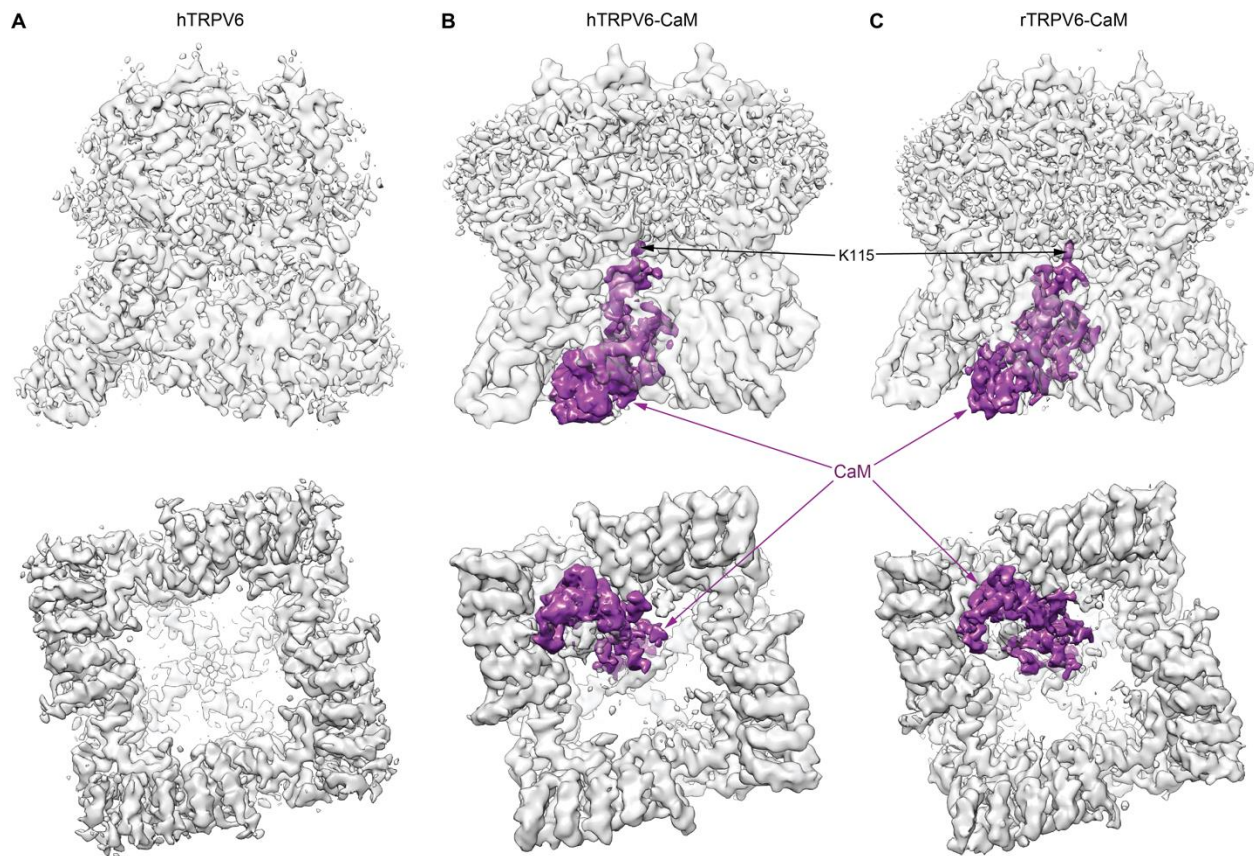


Fig. S2. Comparison of cryo-EM densities for hTRPV6, hTRPV6-CaM, and rTRPV6-CaM.

(A to C) Cryo-EM densities for hTRPV6 (A) PDB ID: 6BO8, hTRPV6-CaM (B) and rTRPV6-CaM (C) viewed parallel to the membrane (top row) and intracellularly (bottom row). The densities for TRPV6 and CaM are semi-transparent-grey and purple, respectively. The densities for CaM residue K115 are indicated.

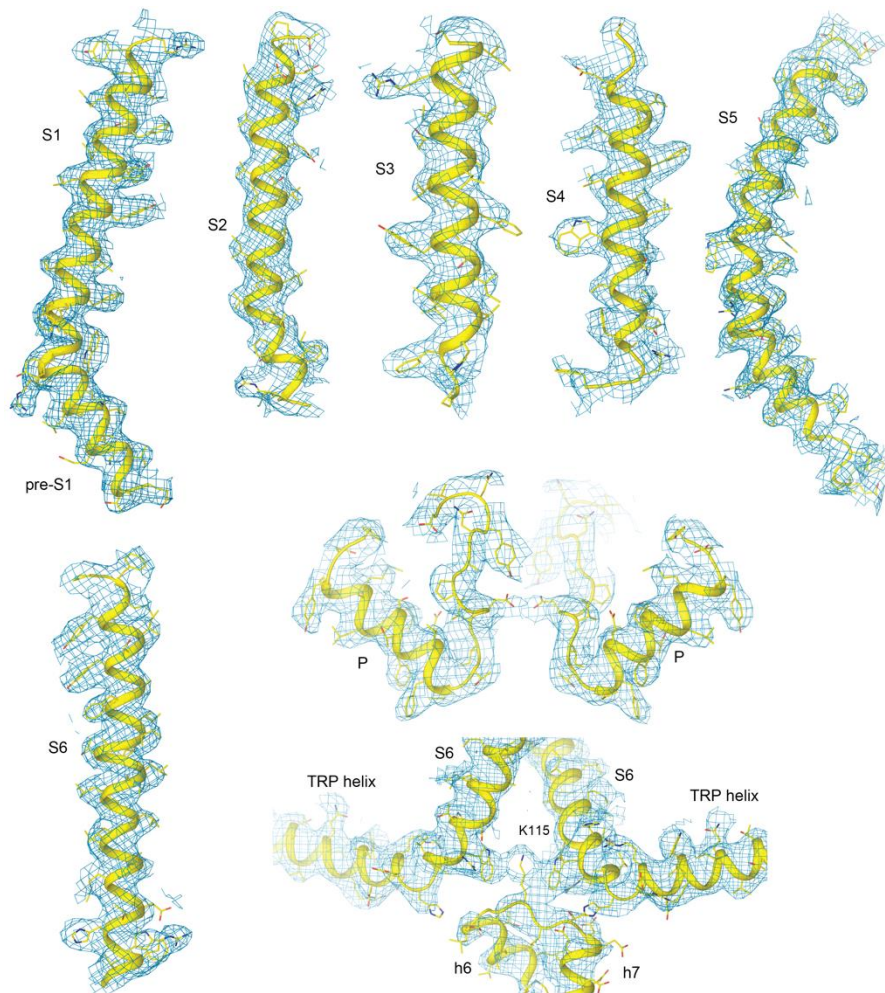


Fig. S3. Cryo-EM density for hTRPV6-CaM. Fragments of the hTRPV6 transmembrane domain and CaM; cryo-EM density is shown at 4σ as blue mesh and the corresponding structural model in yellow.

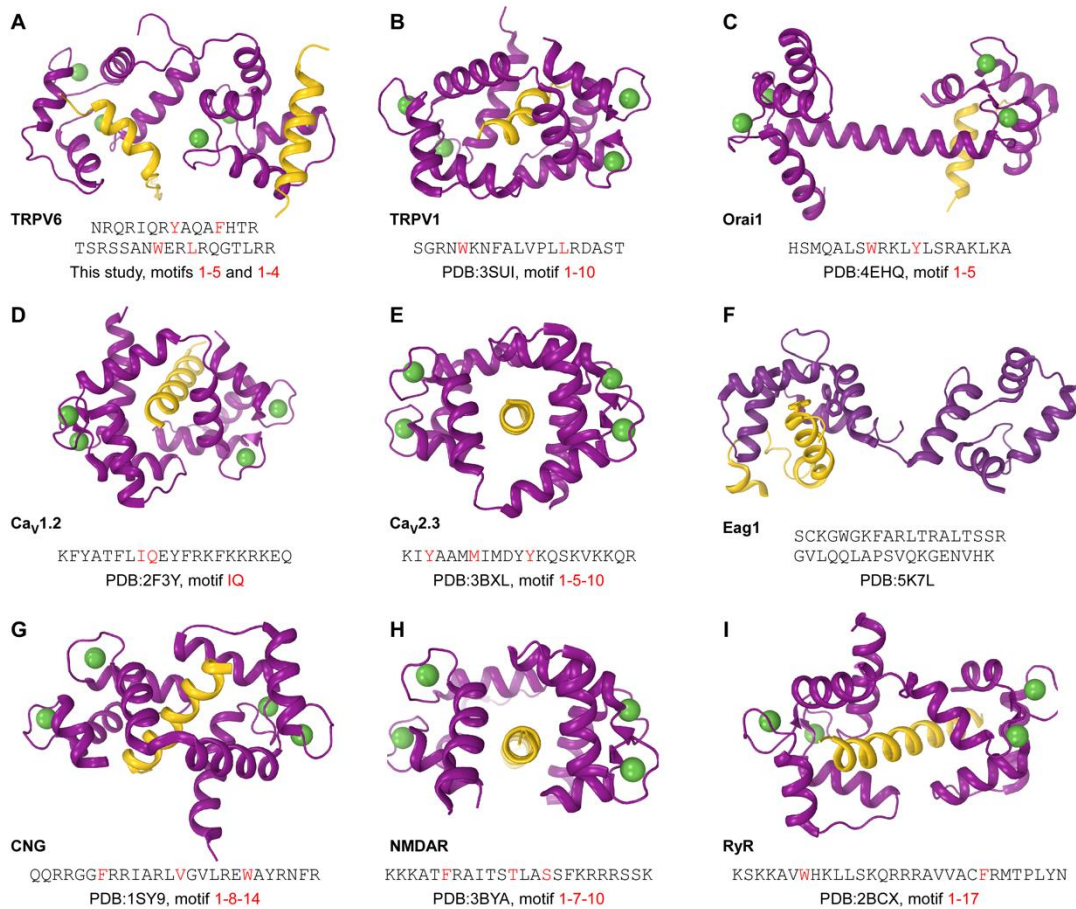


Fig. S4. Structures of CaM bound to ion channel fragments. (A to I) Structures of CaM (purple) bound to fragments (yellow) of the C-terminus of TRPV6 via 1-5 and 1-4 motifs (A) the C-terminus of TRPV1 (PDB ID:3SUI) via a 1-10 motif (B) the C-terminus of Orai (PDB ID:4EHQ) via a 1-5 motif in (C) the C-terminus of CaV1.2 (PDB ID: 2F3Y) via an IQ motif (D) the C-terminus of CaV2.3 (3BXL) via a 1-5-10 motif (E) Eag1 (PDB ID: 5K7L) (F) the C-terminus of the CNG channel (PDB ID: 1SY9) via a 1-8-14 motif in (G) NMDA receptor (PDB ID: 3BYA) via a 1-7-10 binding motif (H) and the C-terminus of the RyR (PDB ID: 2BCX) via a 1-17 motif (I). Amino acid sequences of the binding regions with the binding motif determining residues highlighted in red are shown below the structures. Calcium ions are shown as green spheres.

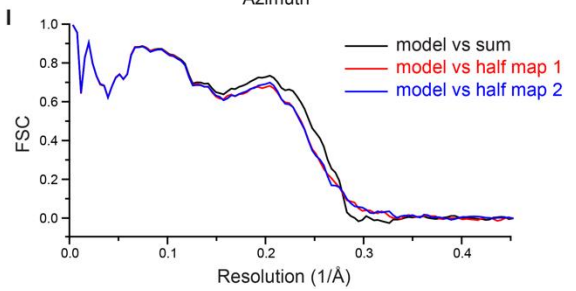
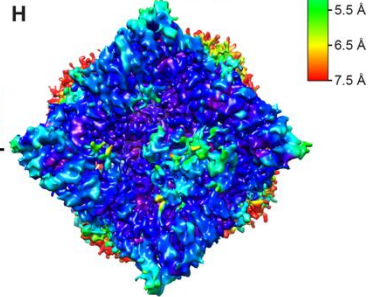
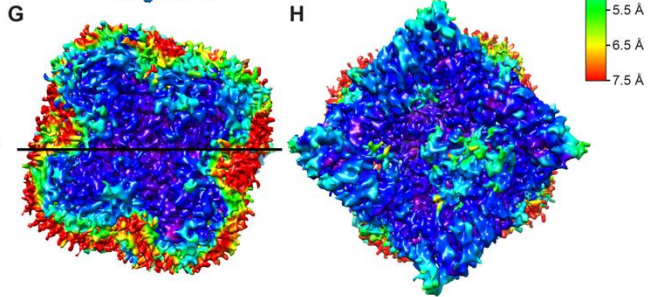
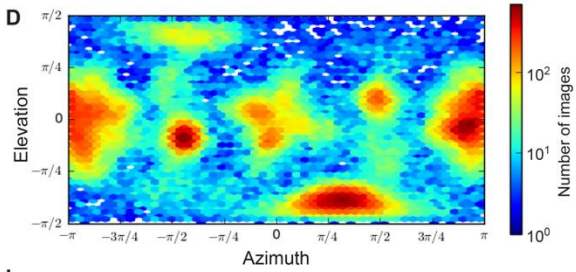
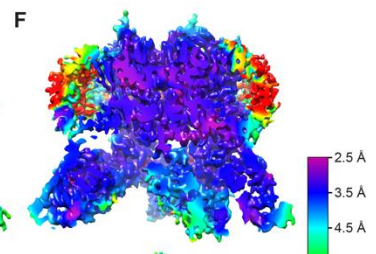
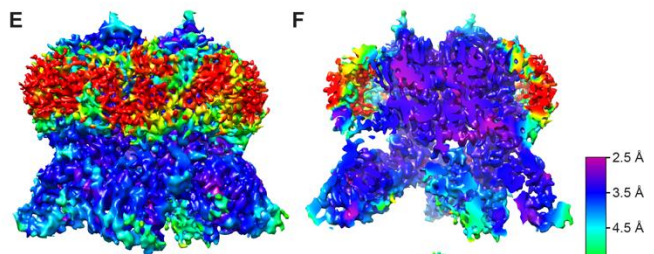
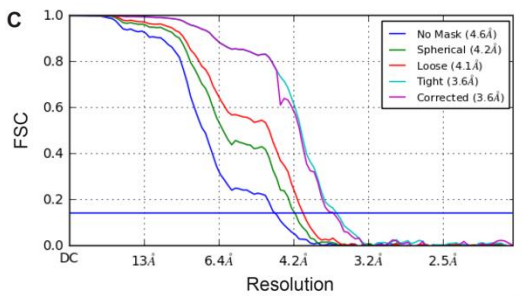
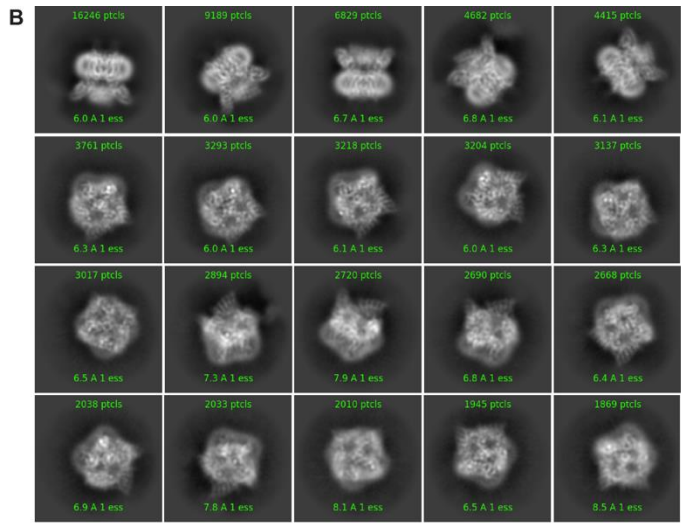
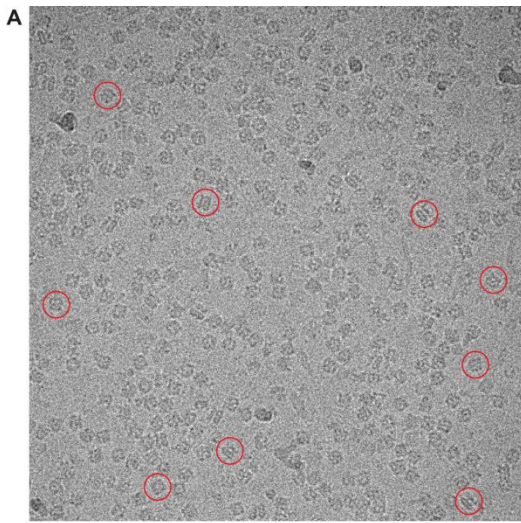


Fig. S5. Overview of single-particle cryo-EM for rTRPV6-CaM. (A) Example cryo-EM micrograph for rTRPV6-CaM with example particles circled in red. (B) Reference-free 2D class averages of rTRPV6-CaM illustrating different particle orientations. (C) FSC curves. (D) Distribution of particle orientations contributing to the final 3.6 Å reconstruction. (E to H) Local resolution mapped on the rTRPV6-CaM density viewed parallel to the membrane (E and F) either in its entirety (E) or coronally halved (F) as well as viewed extracellularly (G) and intracellularly (H). The black horizontal line in (G) indicates the location of the slicing plane in (F). (I) Cross-validation FSC curves for the refined model versus unfiltered half maps (only half map1 was used for PHENIX refinement) and the unfiltered summed map.

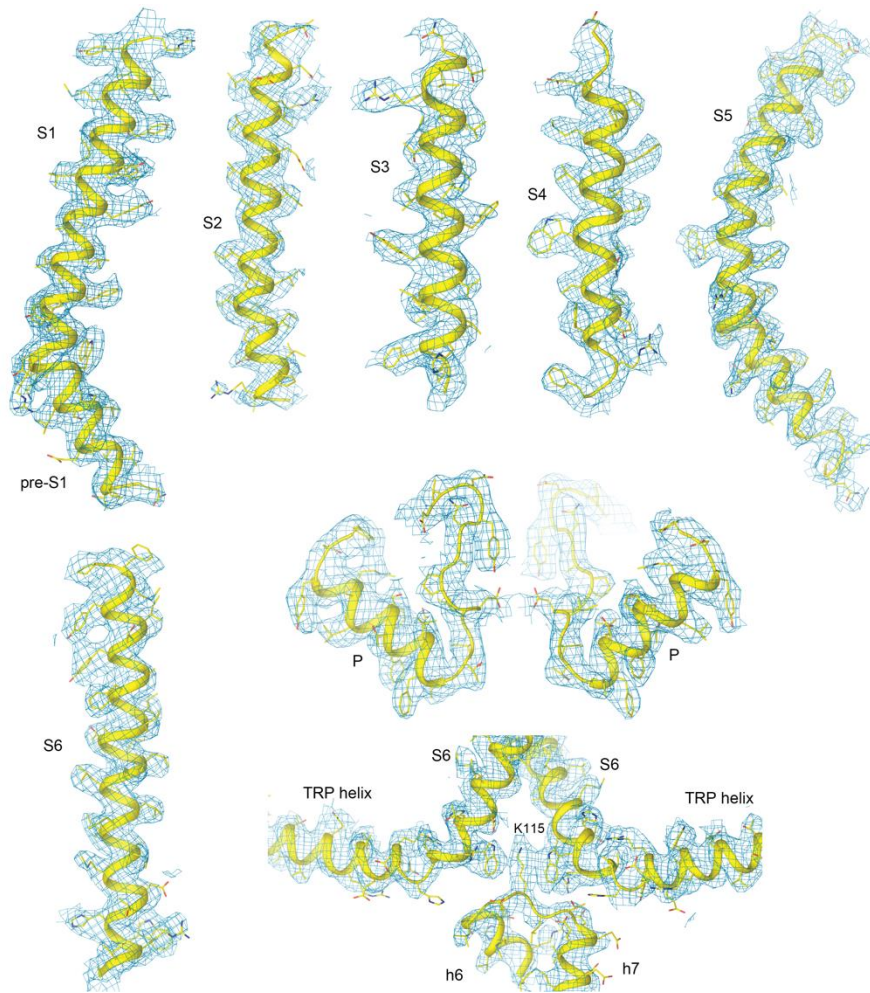


Fig. S6. Cryo-EM density for rTRPV6-CaM. Fragments of the rTRPV6 transmembrane domain and CaM; cryo-EM density is shown at 4σ as blue mesh and the corresponding structural model in yellow.

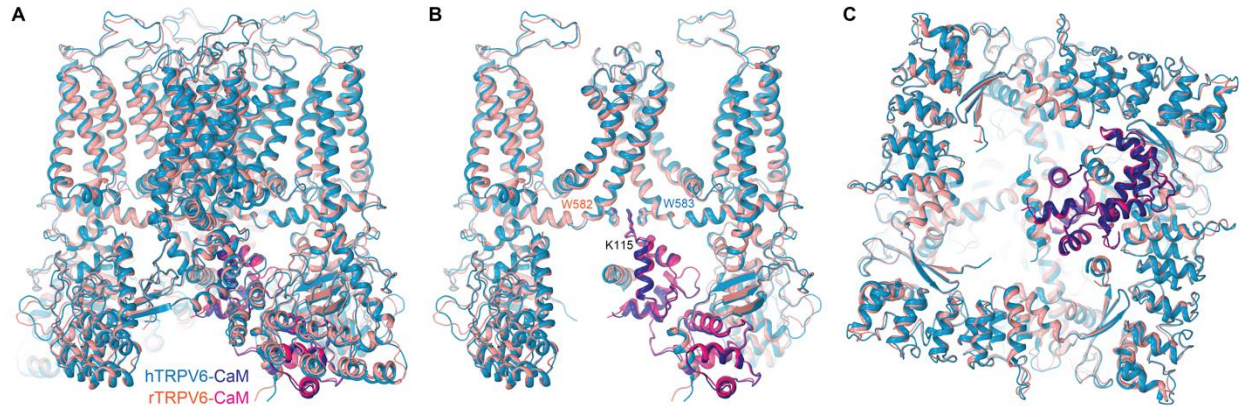


Fig. S7. Comparison of hTRPV6-CaM and rTRPV6-CaM. (A to C) Superposed are hTRPV6-CaM (light and dark blue) and rTRPV6-CaM (salmon and hot pink) viewed parallel to the membrane (A and B) or intracellularly (C). In (B) only two of the four TRPV6 subunits are shown, with the front and back subunits removed for clarity. The residues W583 in hTRPV6, W582 in rTRPV6 and K115 in CaM are shown as sticks.

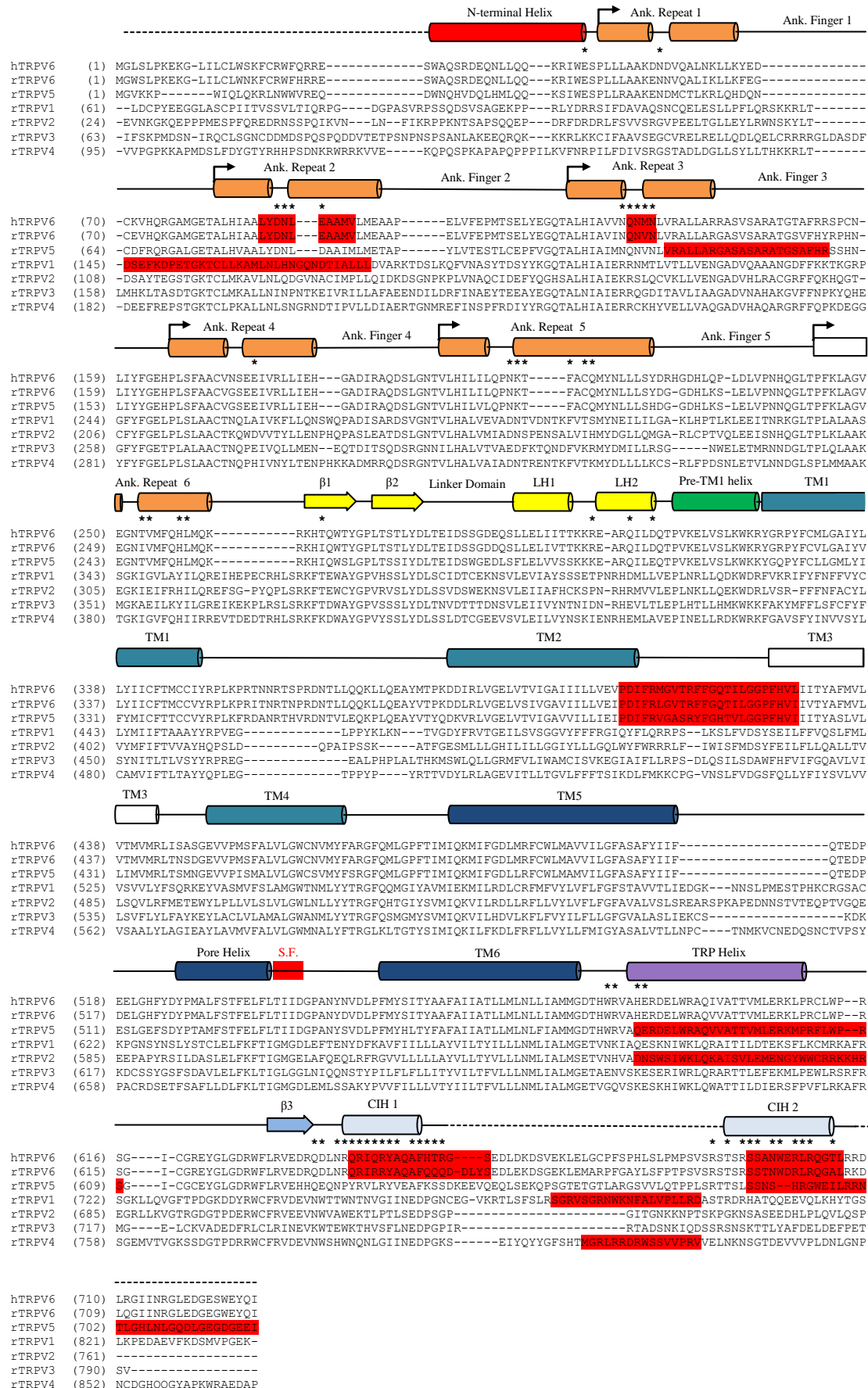


Fig. S8. Sequence alignment of TRPV subunits. Secondary structure elements are depicted above the sequence as cylinders (α -helices), arrows (β -strands) and lines (loops). The red box marks the location of the selectivity filter. Asterisks indicate TRPV6 residues that interact with CaM in hTRPV6-CaM and rTRPV6-CaM structures. The proximal and distal helical portions of the TRPV6 C-terminus that bind CaM are labeled as interacting helices 1 (CIH1) and 2 (CIH2), respectively. Sequences that have previously been shown to interact with CaM (11, 12, 14, 19-23, 26, 42) are highlighted in red. Two TRPV6 peptides have been shown to have nanomolar affinity for CaM, $K_d \sim 43$ nM (23), and $K_d \sim 65$ nM (20).

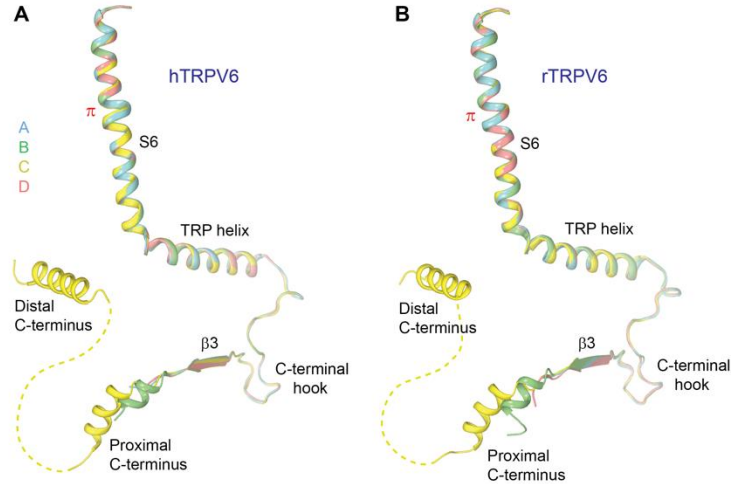


Fig. S9. Superposition of the C termini in different TRPV6 subunits. (A and B)

Superposition of the C-terminal portions of hTRPV6 (A) and rTRPV6 (B) subunits A (cyan), B (green), C (yellow) and D (pink). Dashed lines indicate regions not visible in cryo-EM reconstructions and omitted in the models. Only one distal C-terminal helix is stabilized by CaM binding such that it is visible in the cryo-EM reconstructions and is assigned to subunit C, which also has the most pronounced interaction with CaM via its proximal C-terminus.

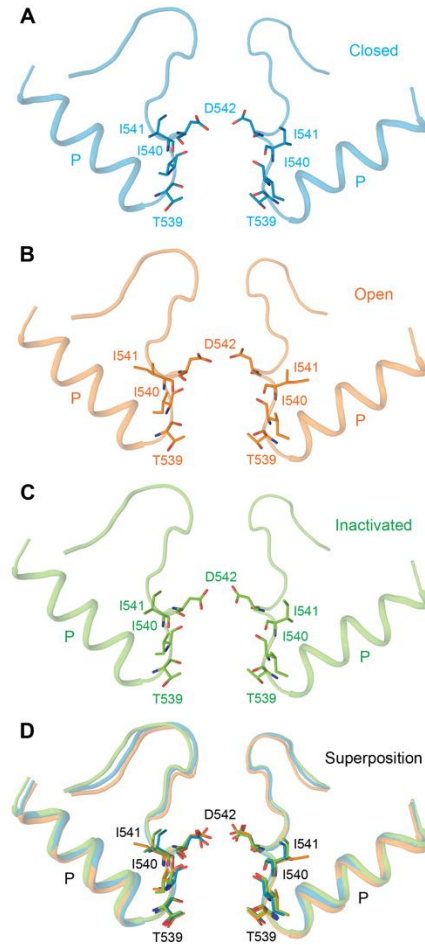


Fig. S10. hTRPV6 selectivity filter from different gating states. (A to C) Structures of the re-entrant P-loops from hTRPV6-R470E (PDB ID: 6BOA) in the closed state (A, blue), hTRPV6 (PDB ID: 6BO8) in the open state (B, orange), hTRPV6-CaM in the inactivated state (C, green). The residues forming the selectivity filter are shown as sticks. (D) Superposition of structures shown in (A to C).

Table S1. Cryo-EM data collection, refinement, and validation statistics.

	hTRPV6-CaM (EMDB-8961) (PDB ID: 6E2F)	rTRPV6-CaM (EMDB-8962) (PDB ID: 6E2G)
Data collection and processing		
Magnification	130,000x	130,000x
Voltage (kV)	300	300
Electron exposure (e ⁻ /Å ²)	55	47
Defocus range (μm)	-1.5 to -3.5	-1.0 to -2.5
Pixel size (Å)	1.08	1.06
Symmetry imposed	C1	C1
Initial particle images (no.)	429,167	507,249
Final particle images (no.)	180,600	111,593
Map resolution (Å)	3.98	3.60
FSC threshold		
Refinement		
Model resolution (Å)	3.98	3.60
FSC threshold		
Map sharpening B factor (Å ²)	-150	-150
Model composition		
Non-hydrogen atoms	21,204	21,108
Protein residues	2640	2637
Ca ²⁺	2	2
B factors (Å ²)		
Protein	178.95	122.62
CaM	295.03	197.03
R.m.s. deviations		
Bond lengths (Å)	0.01	0.006
Bond angles (°)	1.282	1.064
Validation		
MolProbity score	1.90	1.79
Clashscore	4.37	4.34
Poor rotamers (%)	1.4	0.88
Ramachandran plot		
Favored (%)	89.0	89.1
Allowed (%)	10.6	10.9
Disallowed (%)	0.4	0.0